SEMARAK ILMU PUBLISHING

Journal of Advanced Research in Fluid Mechanics and Thermal Sciences

Journal homepage:
https://semarakilmu.com.my/journals/index.php/fluid_mechanics_thermal_sciences/index
ISSN: 2289-7879

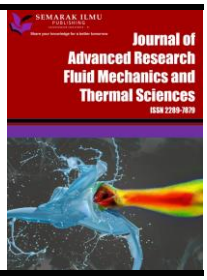

Influence of Sweep Angle on the Surface Pressure of Delta Wing Along Pivot Positions at Hypersonic Mach Numbers

Shamitha[1,2], Asha Crasta[1], Sher Afghan Khan[3,*]

[1] Department of Mathematics, M.I.T.E, Moodabidri & Affiliated To VTU, Belgavi, Karnataka, India
[2] Department of Mathematics, Nitte Meenakshi Institute of Technology Bangalore & Affiliated To VTU, Yelahanka, Bangalore 560064, Karnataka, India
[3] Department of Mechanical Engineering, Faculty of Engineering, IIUM, Gombak Campus, Kuala Lumpur, Malaysia

ARTICLE INFO

Article history:
Received 7 November 2023
Received in revised form 30 March 2024
Accepted 13 April 2024
Available online 30 April 2024

Keywords:
Mach number; surface pressure; delta wing; similitude; strip theory

ABSTRACT

This study focuses on analyzing pressure distribution across the wing surface under different flight conditions. The distribution of surface pressure plays a crucial role in determining the performance of a delta wing. The outcomes of this research will be beneficial for stability assessment and enhancing performance during the aircraft design phase. The paper illustrates the impact of high supersonic Mach numbers, angles of incidence, and specific locations along the three-dimensional delta wing. Strips located at various span-wise positions are treated independently based on a strip theory, which when combined with hypersonic similitude, results in a piston theory. It is important to note that the current theory is only valid when the shock wave remains attached. Viscosity and wave reflection effects have not been taken into account in this particular study. The parameters considered in the study are the Mach numbers (M) in the range 4 to 7. Furthermore, consideration is given to the Angle of Incidence (θ), which varies between 5° to 25°. Along the Wings chord from 0.2 to 1, different points (h) record the pressure results (P2/P1). For numerical simulations, CFD was used, and simulated results at hypersonic Mach numbers matched well with analytical results.

1. Introduction

The exploration of supersonic and hypersonic flow regimes is an integral and essential component of the field of space exploration. Key areas of study encompass space science, long-range weaponry, and space vehicles. Linearization is made possible by assuming that the waves produced by the body's presence are of low intensity. The small disturbance theory and resulting similitude rely on showing that disturbances and gradients are mainly perpendicular to the free stream. It is important to highlight that although this similitude works well for supersonic flow, it does not provide a resolution for hypersonic flow. A fascinating advancement involves expanding the research on supersonic/hypersonic flow beyond slender bodies and low incidences to include non-slender shapes and high incidences.

* *Corresponding author.*
E-mail address: sakhan@iium.edu.my

https://doi.org/10.37934/arfmts.116.2.172191

Hui [1] to build high-speed airplanes and spacecraft, states it is essential to understand how delta wings react in supersonic and hypersonic flows with attached shocks. Hui [2] states that by taking an oscillating wedge, the validity holds for all the supersonic Mach values, the wedge angles, or angles of attack, and, in Hui's opinion, for an oscillating flat plate when there is an associated shock wave. Liu and Hui [3] have developed the pitching delta shock concept proposed by Hui [4]. Lighthill [5] has derived a "Piston Theory" for an oscillating airfoil at high Mach numbers. In line with Lighthill [5] The "Piston Analogy" contrasts a 2-D unstable hypersonic flow with the gas flow in a piston-driven tube. Ghosh uses piston theory and a large incidence of 2-D hypersonic similitude to compute the flow past a wedge and cone. Ghosh and Mistry [6] This concept has been applied up to the order of ¢^{2}. In this case, ¢ represents the angle formed by the shock and the plane that represents the windward surface approximately. The angle created between the body and the shock in the case of a flat surface. Unlike the small disturbance theory, the only other restriction is that the Mach number downstream of the bow shock must be greater than or equal to 2.5 ($M_2 \geq 2.5$). Ghosh [7] developed two similarity criteria as well as a similitude for shock-attached oscillating delta wings at large incidences.

Ghosh developed a unified Supersonic/hypersonic theory for wings in pitch and roll with an attached shock case which has been derived using the unified similarity law. Strip theory is used, where distinct strips are considered independent of each other at various span-wise locations. When combined with similitude, this gives rise to a piston hypothesis [7]. Effects of viscosity and wave reflection have not been considered. Some of the results are compared with those of Liu and Hui [3], Hui *et al.,* [8], and Ghosh [9]. Results have been achieved for a perfect gas moving at hypersonic and supersonic speeds over a wide range of incidences, sweep angles, and Mach numbers. Bashir *et al.,* [10] studied the computational and analytical investigation of aerodynamic derivatives for the oscillating wedge. The CFD simulation with analytical and theoretical validation of various flow parameters for the wedge at supersonic Mach number was obtained by Khan *et al.,* [11]. Aerodynamic coefficients at Mach 6 for the blunt body in the idea of without and with a spike were studied by Kalimuthu *et al.,* [12]. The effect of trailing edge geometry on the aerodynamics of low-speed BWB aerial vehicles was studied by Zuhair and Mohammed [13]. Meng *et al.,* [14] studied the double-cone missile by the combined spike and multi-jet. Shaikh *et al.,* [15] studied the analytical computational analysis of pressure at the nose of a 2D wedge in high-speed flows. Shabana *et al.,* [16] studied the stiffness and damping derivatives of an ogive in the limiting case of Mach number and specific heat ratio. Computational analysis of pressure distribution over a 2D wedge in the supersonic and hypersonic flow regimes is studied by Shaikh *et al.,* [17]. In the current study, the surface pressure distribution along a three-dimensional Delta wing is calculated using Computational Fluid Dynamics (CFD) analysis using ANSYS Workbench. The analysis combines CFD analysis with the parametric study conducted with ANSYS. Consideration is given to Mach values between 4.3 to 7 for wing angles ranging from 5° to 25°. The analysis also involves exploring different pivot locations (h) along the length of the delta wing, ranging from 0.1 to 1. Figure 1 illustrates a wing's geometry.

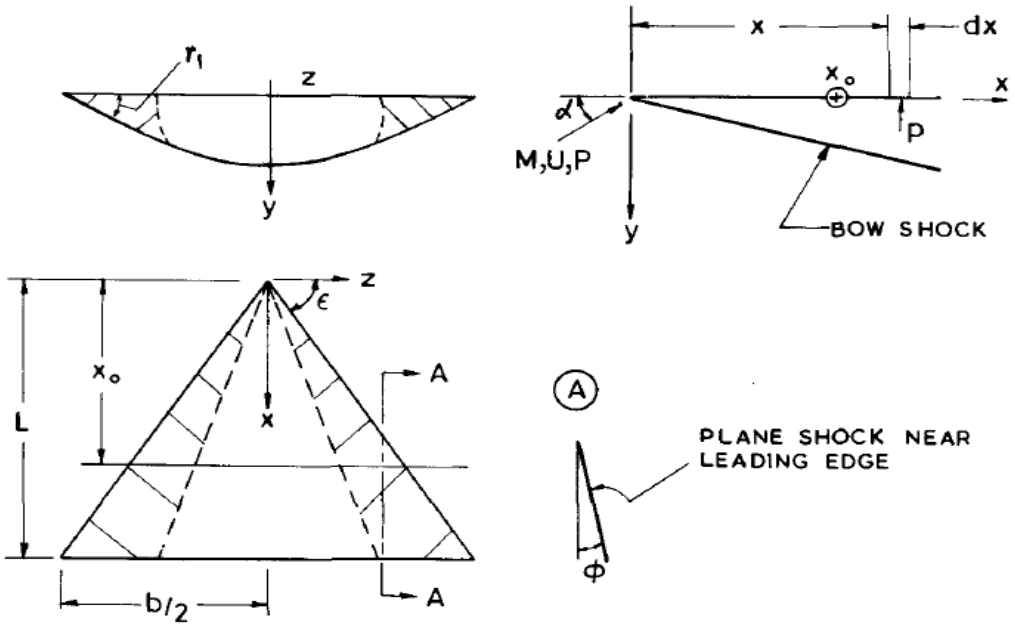

Fig. 1. The Geometry of the wing

Consider a delta wing with a straight leading edge. The Z-axis is perpendicular to the chord inside the wing's plane, whereas the X-axis is aligned along the chord of the wing.

The x-axis equation is provided by z = 0 (1)

The equation of straight L.E is provided by Z = $x\ cot\ \epsilon$ (2)

The equation for an area of wing

Area ABD = $\int_0^C Z\ dx$, Consider $k = \frac{\pi}{C}$

As such, the Ghosh piston theory is utilized taking into account the impact of surface pressure P on the pitching moment and the piston Mach number Mp. Eq. (3) provides the expression for the pressure distribution.

$$\frac{P_2}{P_1} = 1 + C(M_P)^2 + CM_P\sqrt{D + (M_P)^2} \quad (3)$$

where P_1 is the free stream pressure and P_2 is the pressure on the windward surface.

Different span points determine whether a strip is independent. The wing angles and wedge angles are the same. For the time being, 'Mp' and flow deflection are allowed to be high.

$C = \frac{\gamma+1}{4}$, D = $\left(\frac{4}{\gamma+1}\right)^2$

According to a study by Pathan *et al.,* [18], which looked at the base pressure variation in the inside and outside flows as determined by CFD analysis, the quickly increasing inner and outside flows are almost identical in the base region of the flow field. Research was conducted on base pressure regulation techniques, which were analyzed by Pathan *et al.,* [18,19], Shaikh *et al.,* [20], and Khan and Rathakrishnan [21]. Kanaani *et al.,* [22] investigated the optimization of longer duct length in

suddenly expanded flows. According to the literature, no research has been done on the surface pressure over the entire Delta wing.

In the current research, an investigation is conducted into the surface pressure distribution along the Delta wing. This is achieved by modeling the surface pressure along the wing's pivot location using Computational Fluid Dynamics (CFD) analysis and varying the flow parameters. The surface pressure of the wing is solved numerically for supersonic Mach numbers of 4.3, 4.8, 5.5, and 7. Along the delta wing's length, the location (h) varies from 0.2 to 1.0, and the angle of incidence (θ) from 5° to 25°.

2. Methodology

2.1 CFD Analysis

Fluent and an academic ANSYS Workbench license are used for the Computational Fluid Dynamics (CFD) investigation in this work. Mesh along with modelling is done with ANSYS Workbench, and analysis and post-processing are done with ANSYS Fluent. Numerical findings are exact and accurate when the structured mesh is used. Angles of incidence of 5°, 10°, 15°, 20°, and 25° are taken into account along with a range of Mach values of 4.3, 4.8, 5.5, and 7. When performing the CFD analysis for a weak solution with the attached shock wave.

2.1.1 Modelling

With the ANSYS design Modeler, all axisymmetric geometries with different angles of incidence are modeled. Figure 2 illustrates the geometry of the wing and enclosure. Each geometry takes into consideration the various incidence angles, which are 5°, 10°, 15°, 20°, and 25°. The Bottom View, 3D Geometry isometric view, and delta wing with angle of attack of 5°, 10°, 15°, 20°, and 25°, respectively, are showcased in Figure 2(a) and Figure 2(b), Figure 2(c), Figure 2(d), Figure 2(e), and Figure 2(f).

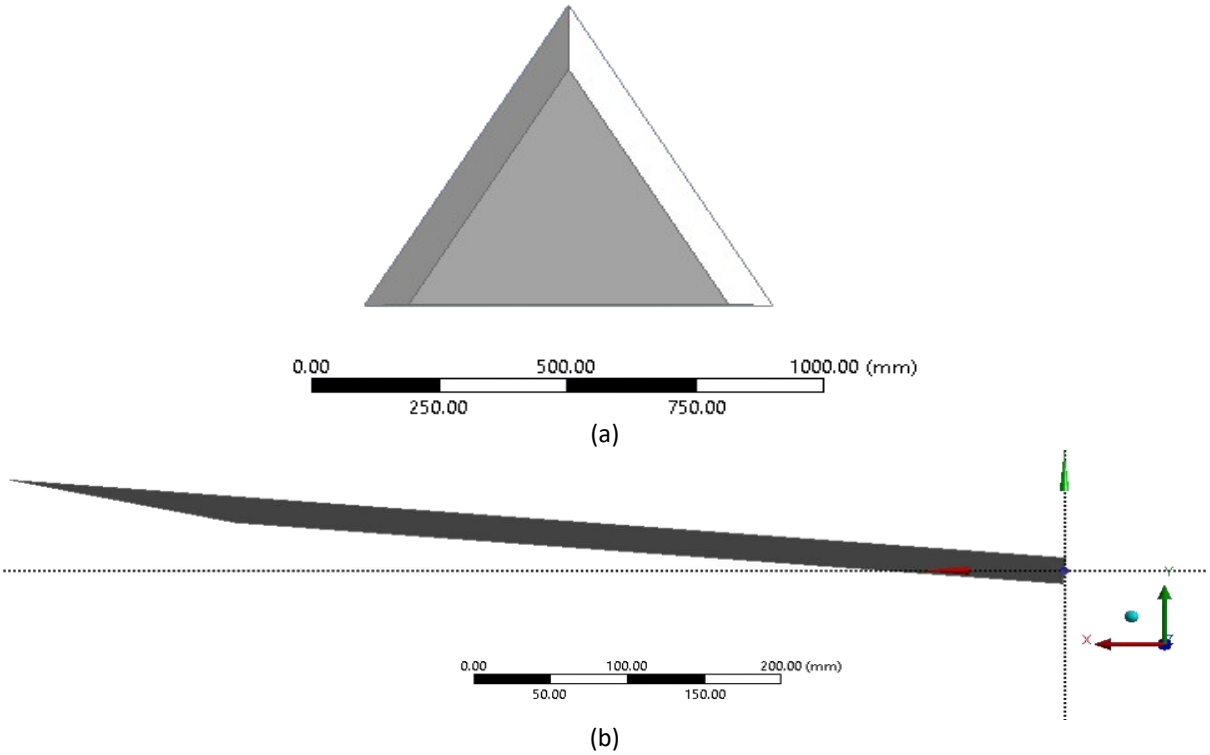

(a)

(b)

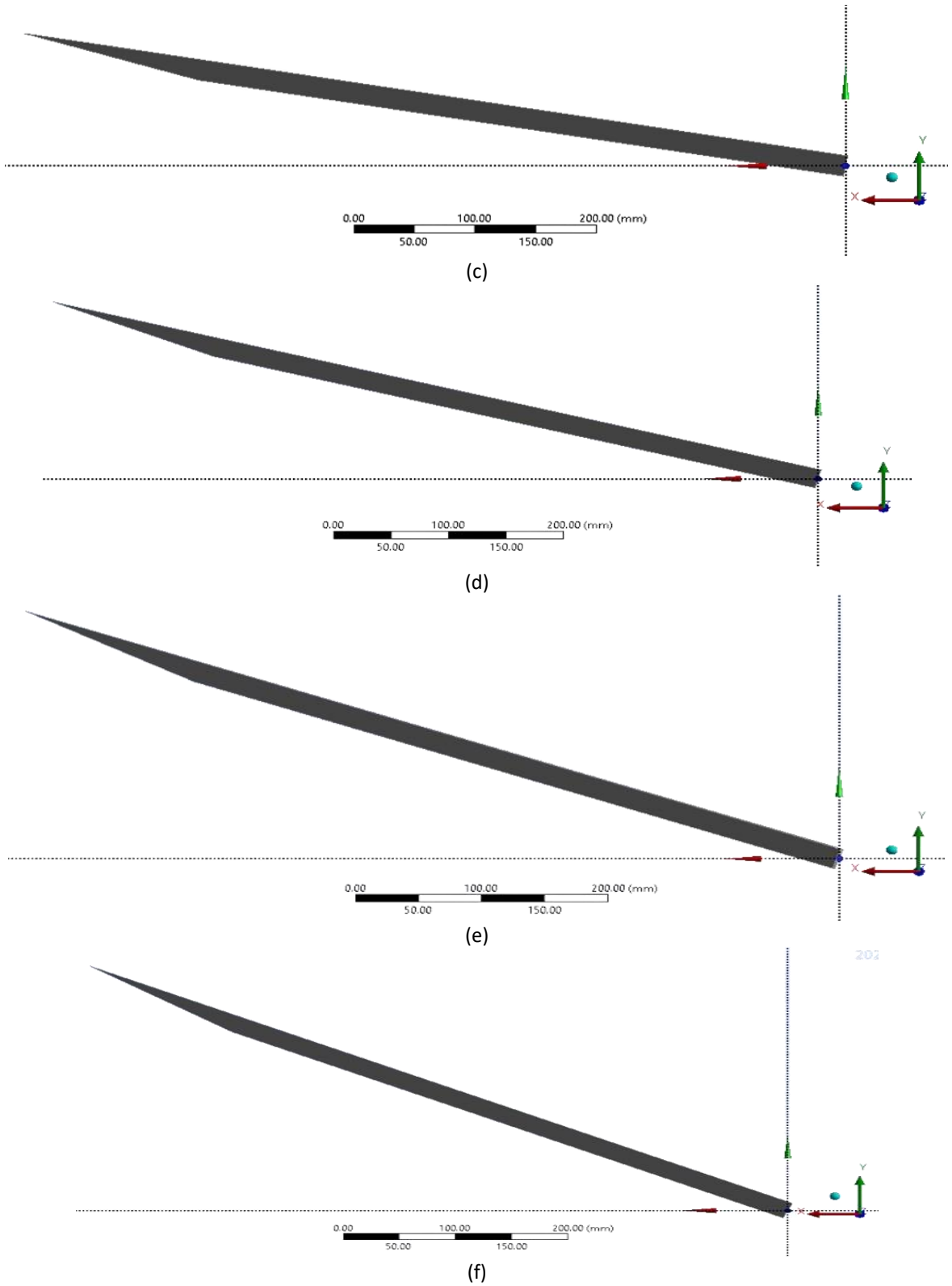

Fig. 2. (a) Bottom View, 3D Geometry isometric view, (b) Delta wing with angle of attack = 5°, (c) Delta wing with angle of attack = 10°, (d) Delta wing with angle of attack = 15°, (e) Delta wing with angle of attack = 20°, (f) Delta wing with angle of attack = 25°

2.1.2 Meshing

In numerical simulations such as Computational Fluid Dynamics (CFD), a grid independence test is an essential step to make sure that the mesh size has no appreciable impact on the results. It assists in figuring out the ideal mesh size that yields trustworthy outcomes at a reasonable computational cost. A grid independence test with a range of mesh sizes from 10 mm to 400 mm was conducted for a wing angle of 15° and a Mach number of 7. The number of elements and nodes for the mesh, which has sizes ranging from 400 mm to 10 mm, is displayed in Table 1.

Table 1
The number of mesh elements with different element sizes is used for the grid independence test

Size of Mesh Element in mm	Number of Mesh Nodes	Number of Mesh Elements
400	350937	304728
300	386031	335201
200	421124	365674
150	505349	438808
100	589574	511943
50	884361	767915
25	1768722	1535829
10	5306167	4607487

Figure 3 presents the results of the grid independence test. It is wise to select this mesh size as the ideal one for additional CFD analysis. Conducting effective and dependable simulations requires balancing computational cost and accuracy, which is why a 50 mm mesh size is chosen. The findings show stability at a mesh element size of 50 mm, confirming that it is appropriate to take into account more CFD analysis.

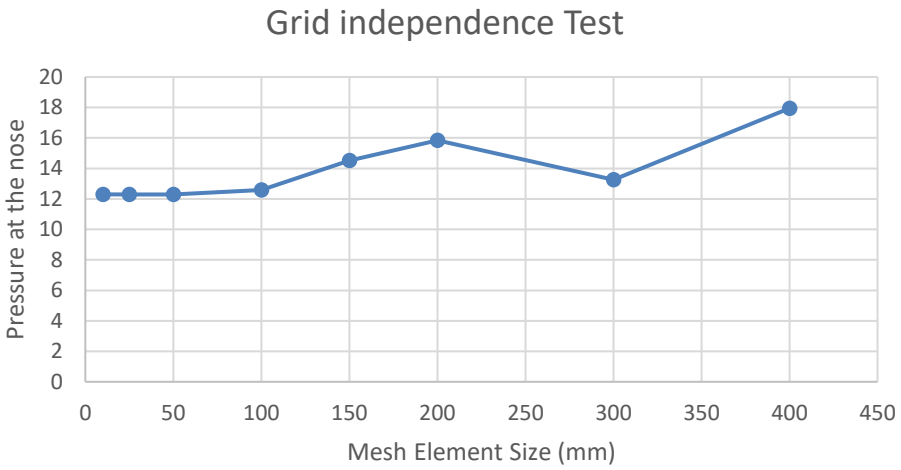

Fig. 3. Grid independence test

Figure 4(a) illustrates the comprehensive 3D meshed model with enclosure, while Figure 4(b) provides an expanded view of the wing geometry. The complete meshing configuration of a delta wing is depicted in a closed view for the entire setup.

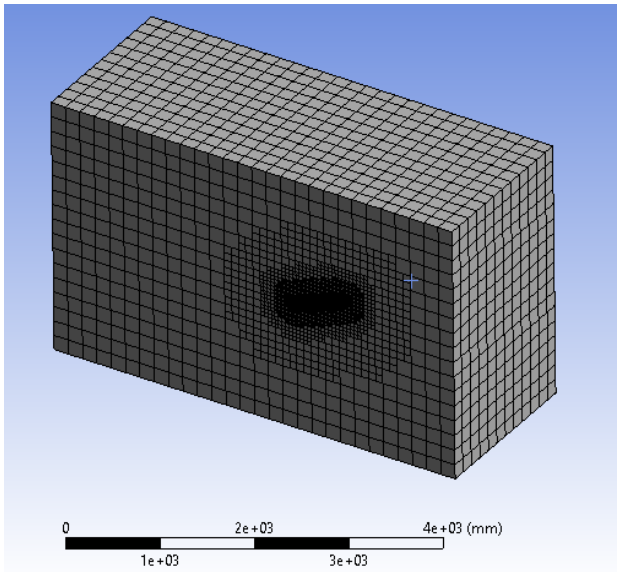

(a) Comprehensive 3d meshed model

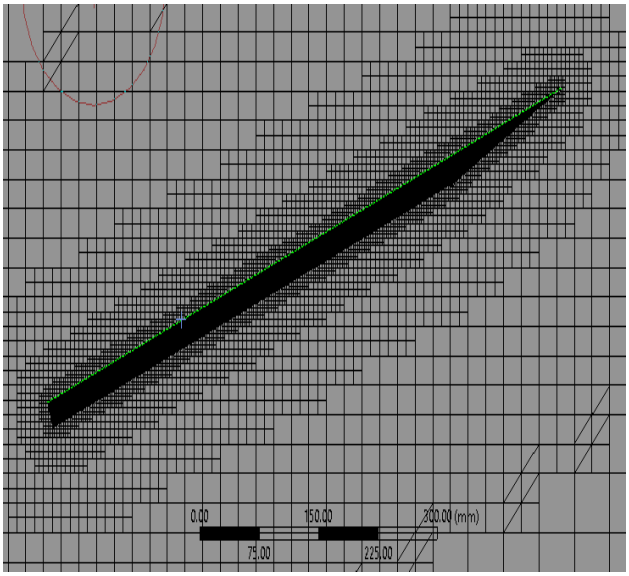

(b) Meshed configuration of a delta wing in a closed view

Fig. 4. (a) Complete geometry, (b) Meshed configuration of a delta wing

2.1.3 CFD analysis

The comprehensive CFD analysis encompasses all possible parameter combinations. Once boundary conditions are set, the solution undergoes initialization and iterates for a minimum of 10,000 cycles, with resolution achieved after 1000 iterations in multiple cases. The widely recognized k-epsilon turbulent model is employed, accompanied by two additional transport equations illustrating turbulent flow characteristics. The parameters that characterize the inlet and outflow boundary conditions are the velocity intake and pressure outlet, respectively. The velocity is multiplied by the Mach number to get the inlet velocity. When the pressure at the outflow is zero, air pressure is the outcome. Because the flow is supersonic and compressible, a density-based solution is applied using the EASY approach technique.

2.1.4 The corroboration of current work through literature

The validation process, which determines the reliability and validity of our simulation results, is an essential component of CFD analysis. CFD results validate the applicability of the simulations to real-world circumstances, as illustrated in Figure 5, by providing evidence of the models' correctness when they agree well with data from the literature. The pressure on the oscillating wing has been examined and calculated by Zuhair and Mohammed [13] in connection to piston Mach number = 5.5. The overall agreement between the current research activity and the analytical investigation's conclusions regarding pressure variation is shown in Figure 5.

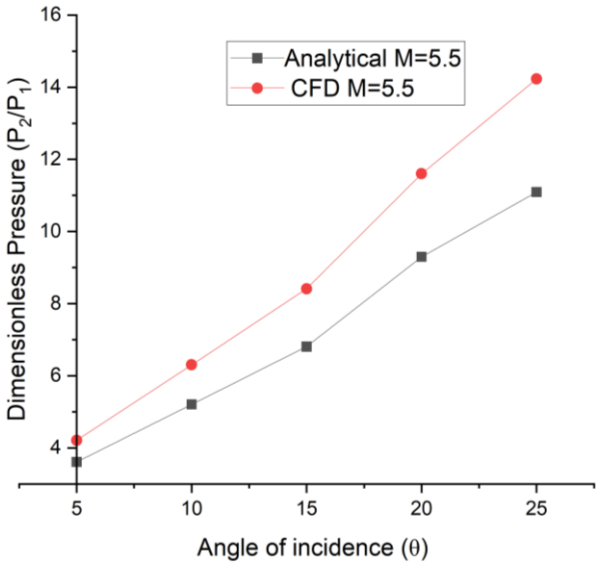

Fig. 5. Assessment of the dimensionless pressure fluctuation using CFD and analytical research at M=5.5

2.2 Pressure Contours' Results

Figure 6 illustrates graphically how the Mach angle decreases as the Mach number increases. Additionally, the same figure shows pressure contours for different incidence angles and Mach numbers. Notably, the wing area expands with a higher wing angle. The outcomes underscore that, at a constant wing angle, the Mach angle diminishes as the Mach number increases.

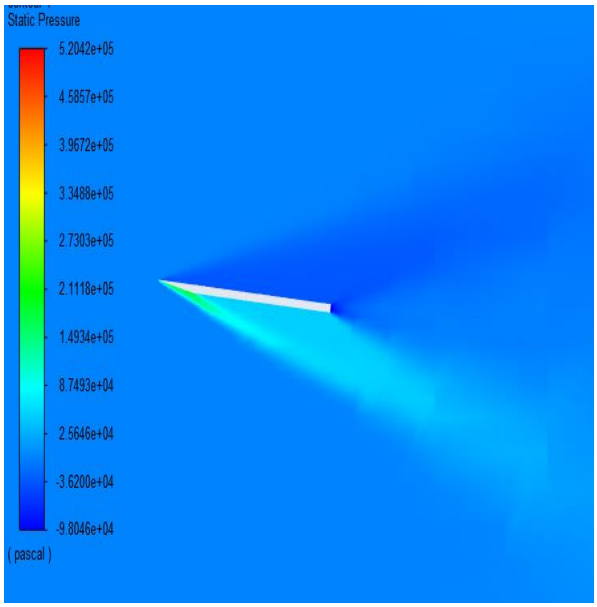

(a) M=4.3, θ=5°

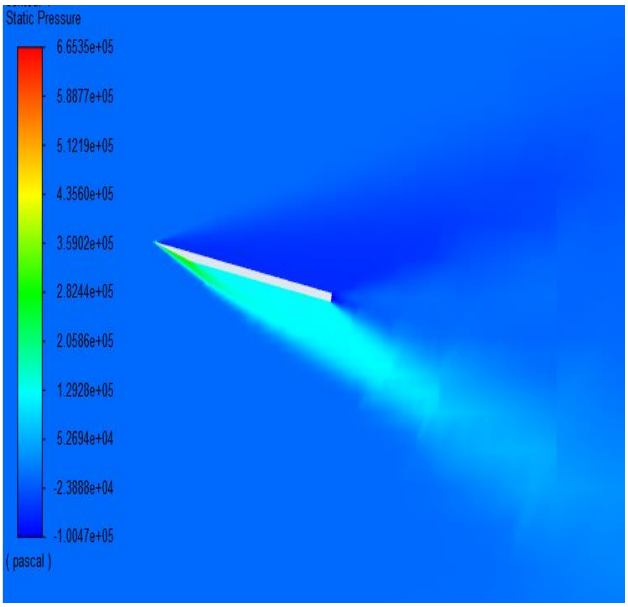

(b) M=4.3, θ=10°

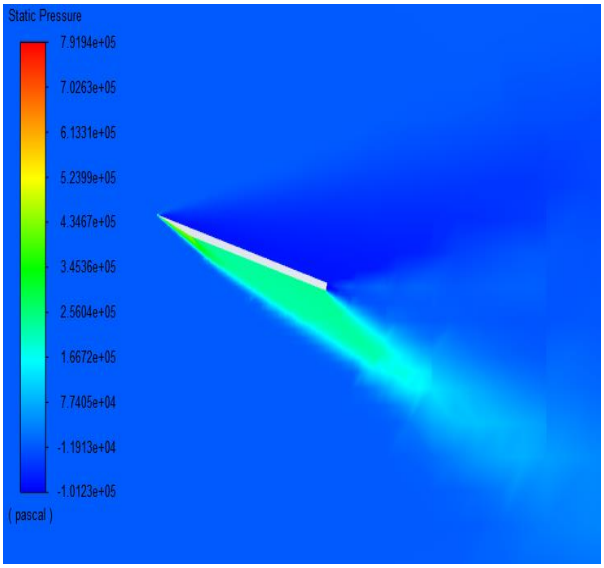

(c) M=4.3, θ=15°

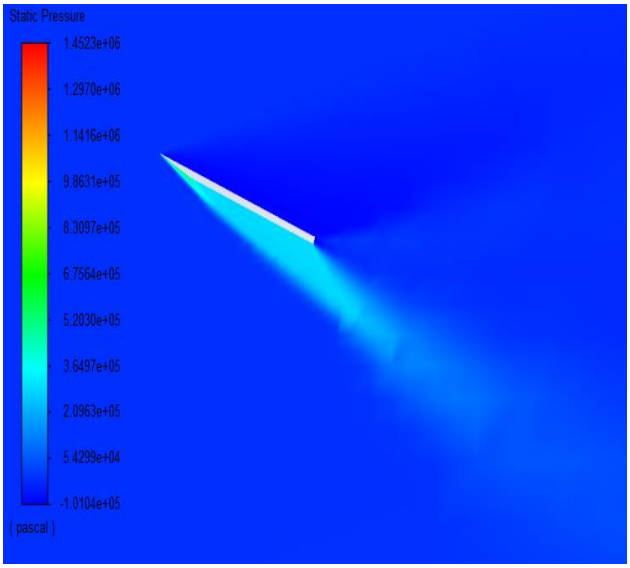

(d) M=4.3, θ=20°

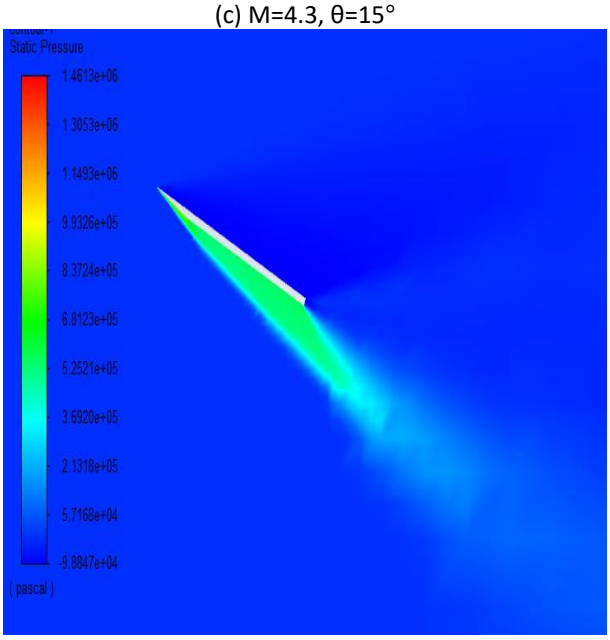

(e) M=4.3, θ=25°

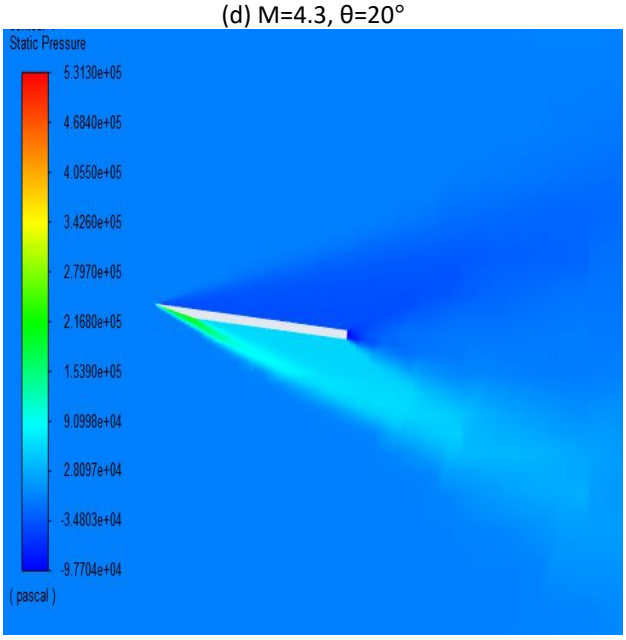

(f) M=4.8, θ=5°

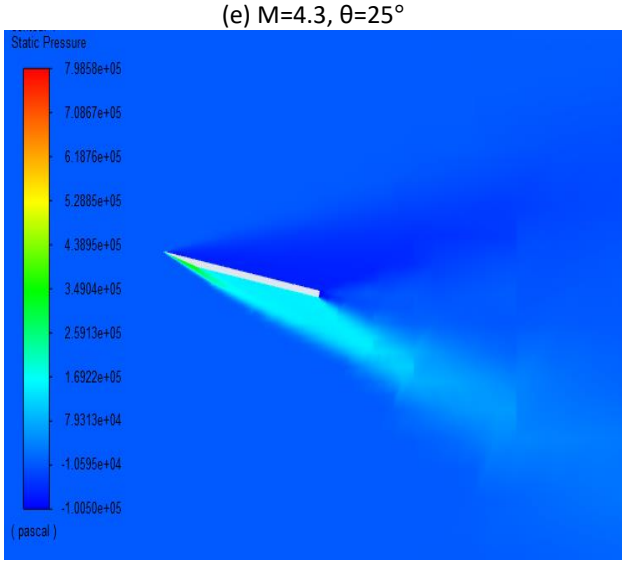

(g) M=4.8, θ=10°

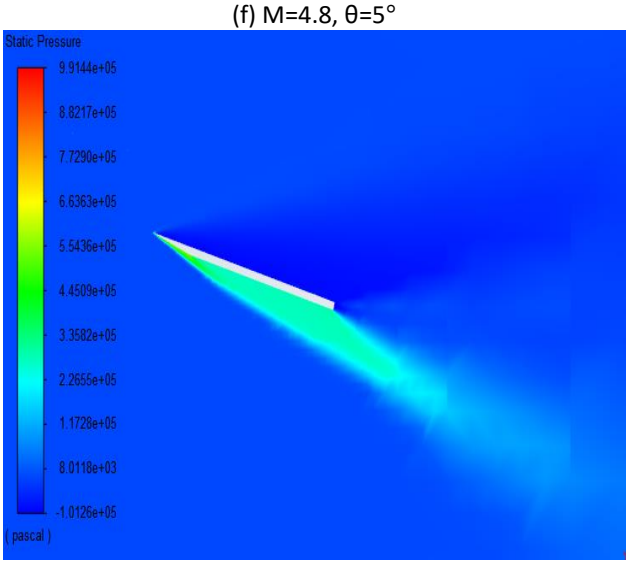

(h) M=4.8, θ=15°

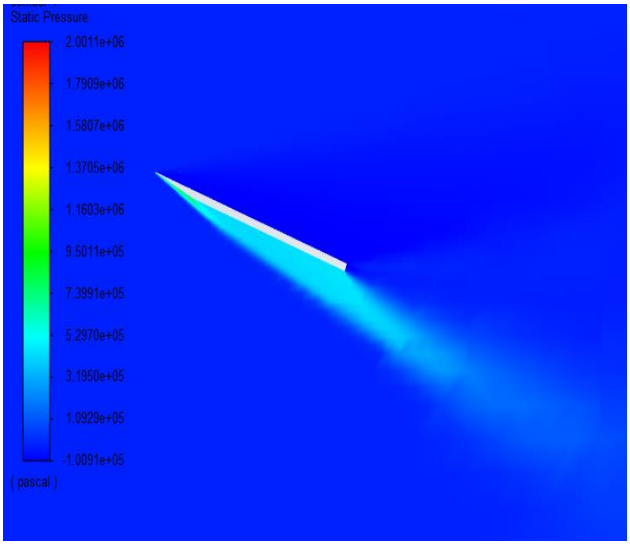

(i) M=4.8, θ=20°

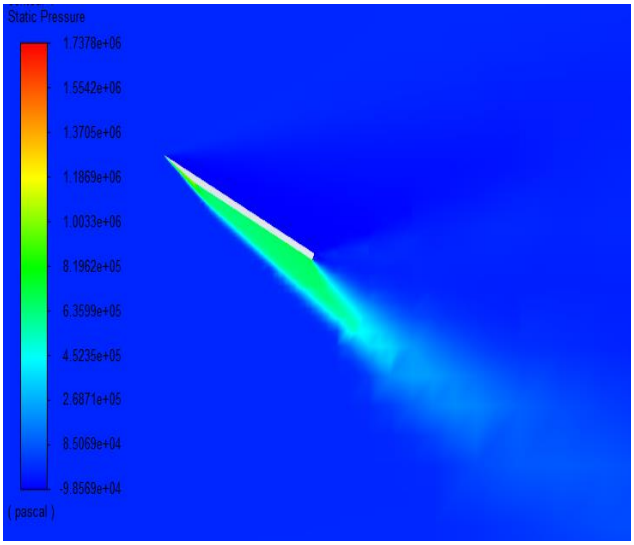

(j) M=4.8, θ=25°

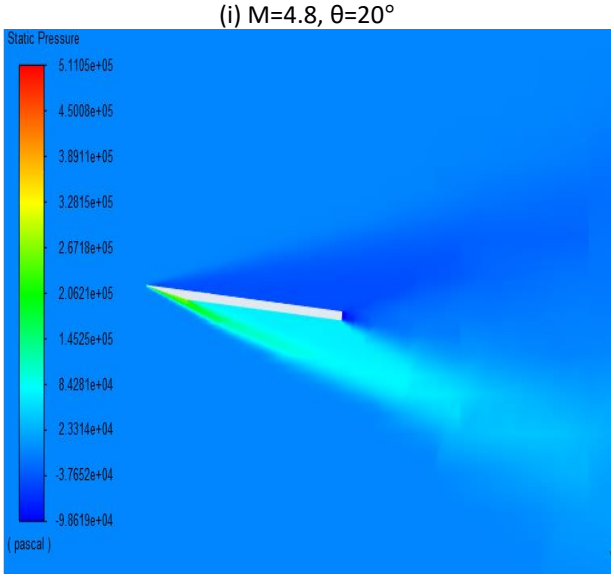

(k) M=5.5, θ=5°

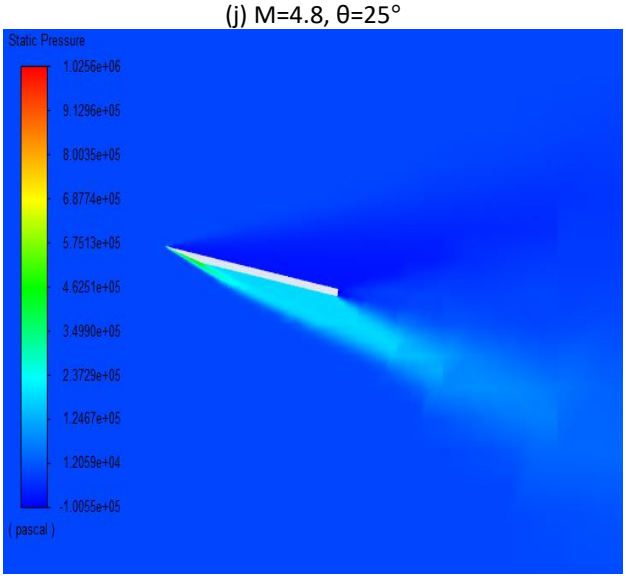

(l) M=5.5, θ=10°

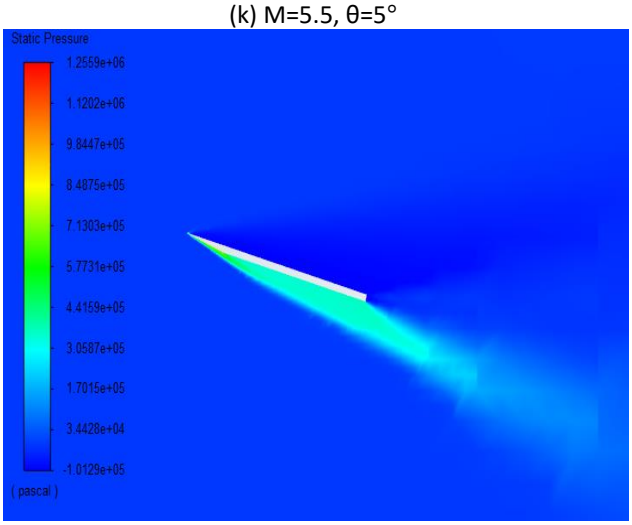

(m) M=5.5, θ=15°

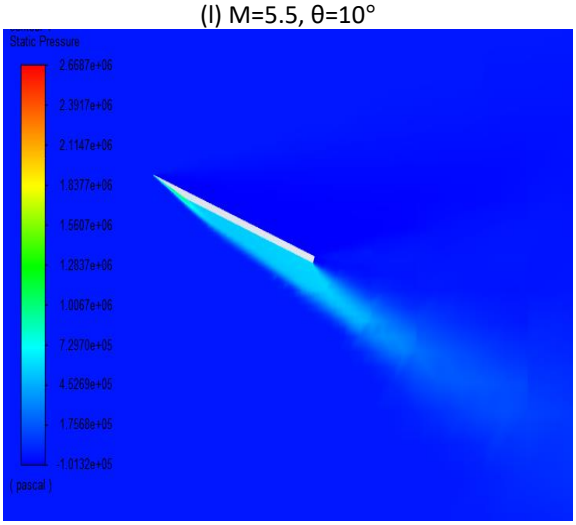

(n) M=5.5, θ=20°

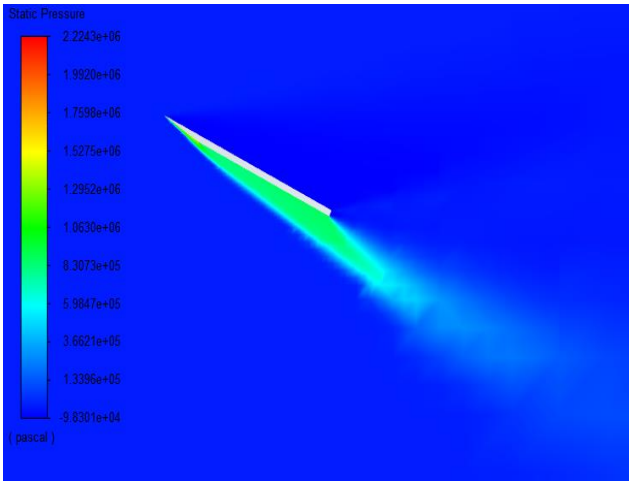

(o) M=5.5, θ=25°

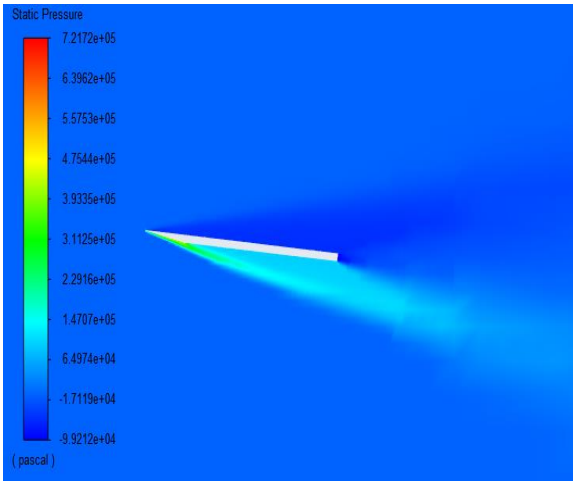

(p) M=7, $\theta = 5°$

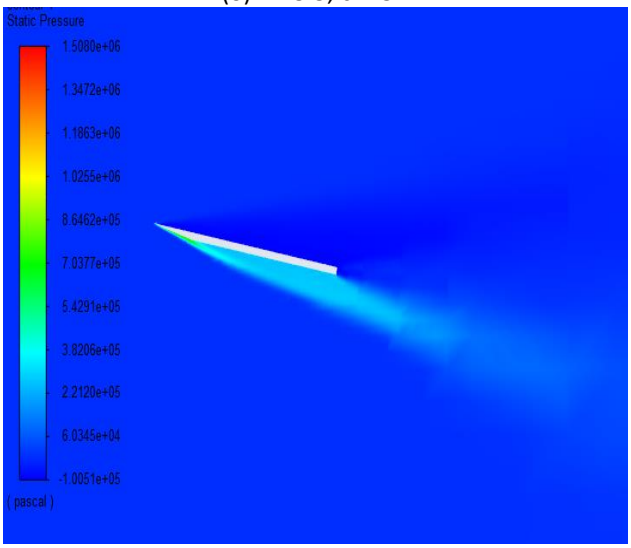

(q) M=7, $\theta = 10°$

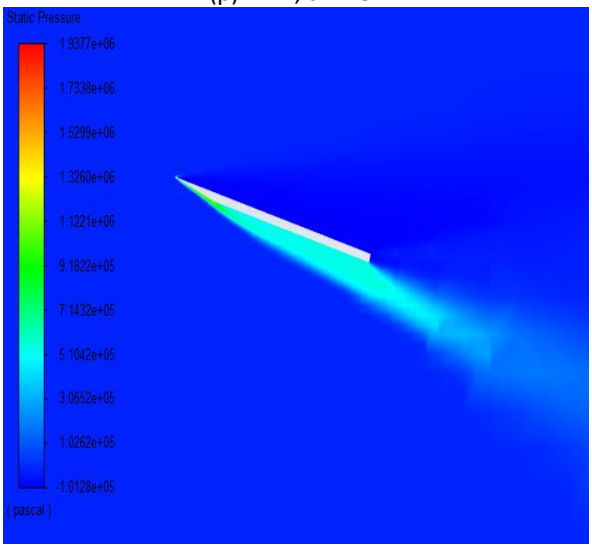

(r) M=7, $\theta = 15°$

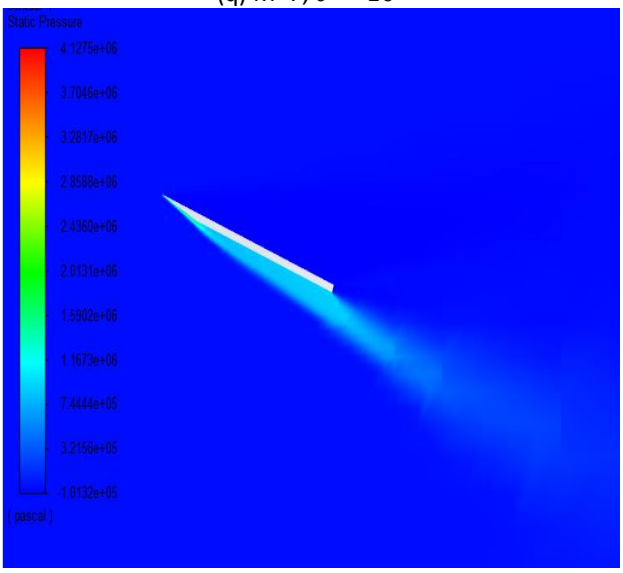

(s) M=7, $\theta = 20°$

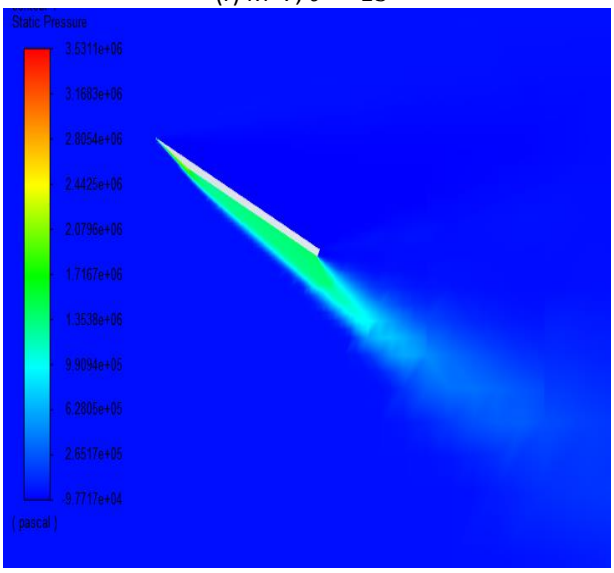

(t) M=7, $\theta = 25°$

Fig. 6. Pressure contours for different incidence angles and Mach numbers

3. Results and Discussion

3.1 Mach Number Plots for the Principal Effects of Dimensionless Static Pressure

The Mach number's principal impact on the dimensionless static pressure (P_2/P_1), or ratio of atmospheric pressure (P_1) at the wing's nose to pressure at a point (P_2), is depicted in Figure 7. The figure also accounts for the average pressure values in each case. The results indicate that an increase in Mach number leads to a corresponding rise in static pressure at the nose of the delta wing.

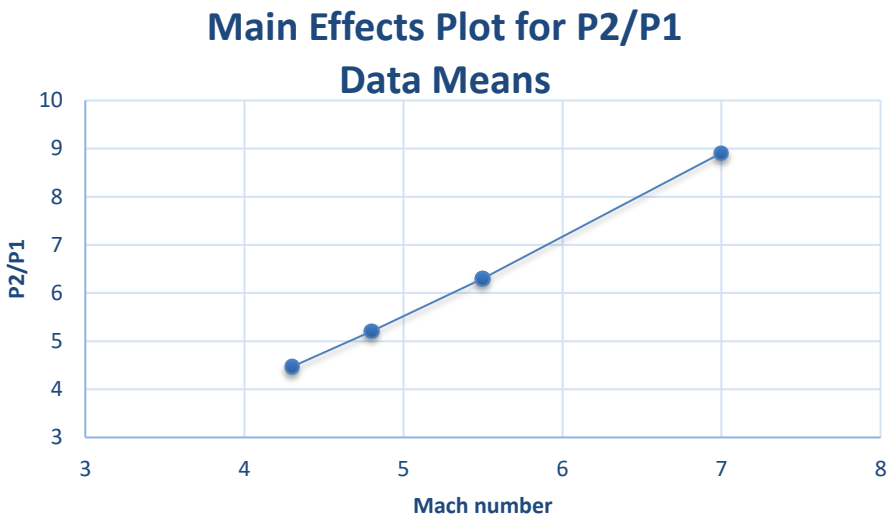

Fig. 7. Mach number's primary impact on the pressure at the wing's nose

3.2 Principal Impact Plots for Dimensionless Static Pressure: Angle of Incidence

Figure 8 illustrates the primary impact of the angle of incidence on the dimensionless static pressure (P_2/P_1) at the wing's nose. The results demonstrate that an increase in the angle of incidence is accompanied by an increase in the static pressure at the wing's nose.

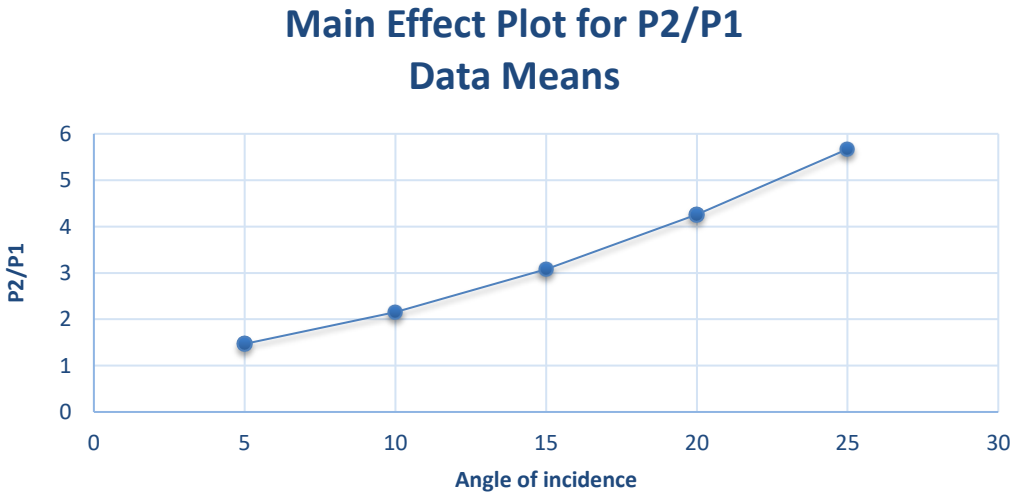

Fig. 8. The primary impact of the angle of incidence on the pressure at the wing's nose

3.3 The Following Impacts on Dimensionless Static Pressure are Present Along the Wing's Length

Figure 9 shows the main effect of position (h) along the length of the wing plots for dimensionless static pressure. According to the data, the static pressure drops from 0.2 to 0.4. Due to pressure, the pressure will decrease from a place 0.4 to 0.6 from location 0.4, after which it will remain stable.

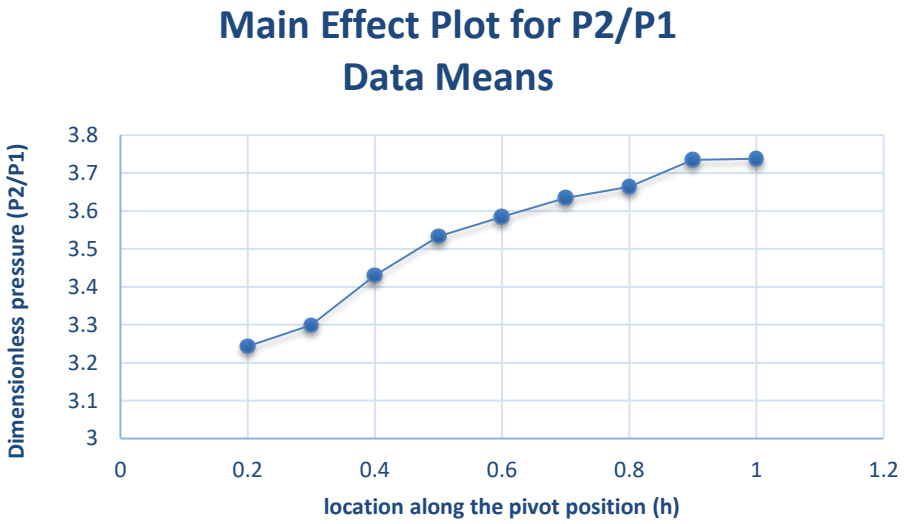

Fig. 9. Main effect of location along the pivot position vs. dimensionless pressure (P_2/P_1)

3.4 The Surface Pressure for a Constant Mach Number at Different Points Along The Wing's Length

The pressure over the pivot position (h) has been analyzed using CFD using ANSYS software, and graphs have been plotted at a constant Mach number. By dividing the static pressure data by air pressure, dimensionless pressure values are produced.

The fluctuation in dimensionless static pressure vs pivot position over the length of the wing at different angles of incidence, with a constant Mach number of M = 4.3, is displayed in Figure 10. The findings strongly imply that as the angle of incidence rises, the pressure keeps rising. In addition, the pressure decreases at all incidence angles from 0.2 to 0.4. The pressure was constant from position 0.5 to 1 at incidence angles of 5°, 10°, and 15°. For the values of the angle of incidence between 20° and 25°, there is a rise in pressure then 0.5 onwards its stable. There are also slight variations in pressure observed following the position between 0.9 and 1.

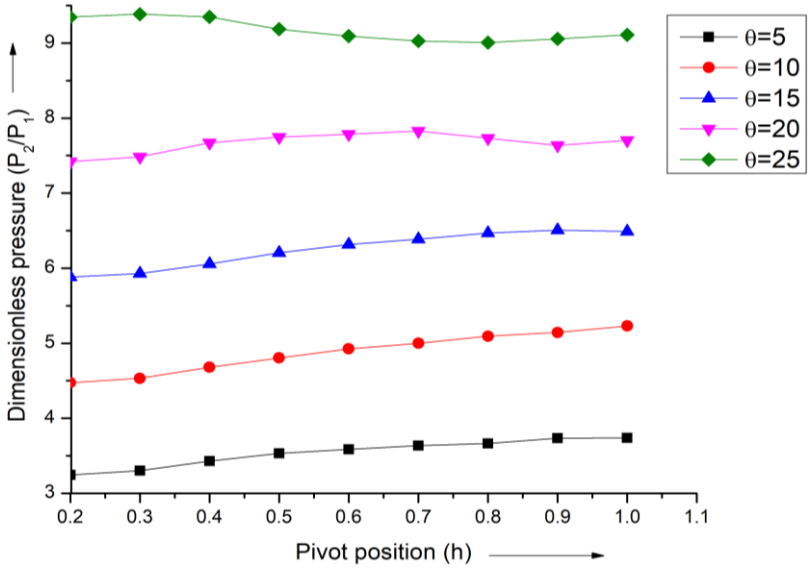

Fig. 10. Dimensionless pressure variation along the pivot position (h) at M = 4.3

Figure 11 illustrates the variation in the dimensionless static pressure vs pivot point along the wing's length for various angles of incidence, with a constant Mach number of M = 4.8. The results show that pressure rises continuously with an increase in the angle of incidence. Additionally, it is observed that for an angle of 5° to 20°. Furthermore, it is noted that the pressure increases from position 0.2 to 0.5 at angles ranging from 5° to 20°. After location 0.5, the pressure remains constant.

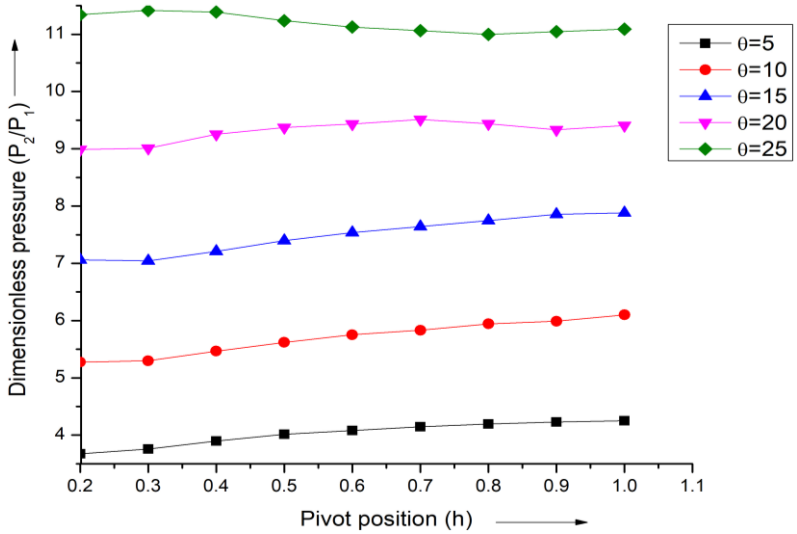

Fig. 11. Dimensionless pressure variation along the pivot position (h)) at M = 4.8

Figure 12 illustrates the fluctuation in the dimensionless static pressure against pivot location along the 3D wing's length for various incidence angles, with a constant Mach number (M = 5.5). According to the findings, the pressure increases from 0.2 to 0.5 along the wing's length for an angle of incidence of 5^0 degrees. It is noted that for all angles of incidence, pressure remains constant between 0.5 and 1.0. Between positions 0.2 and 0.4, there is a marginal pressure variation that shows a reduction for angles 20° and 25°.

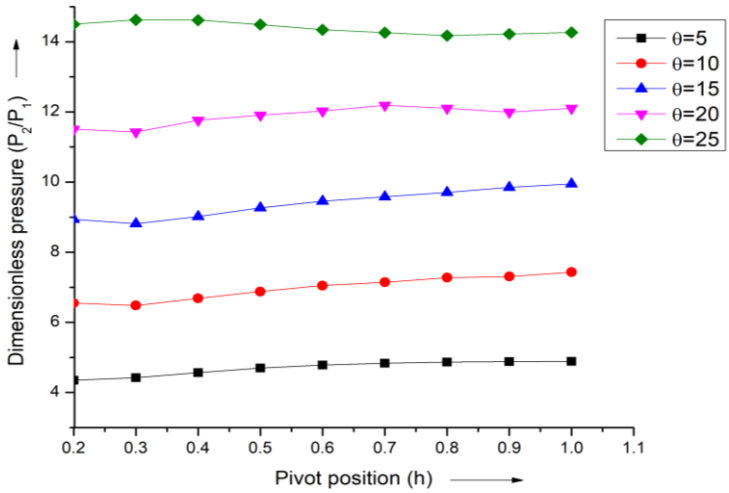

Fig. 12. Dimensionless pressure variation along the pivot position (h) at M = 5.5

Figure 13 displays the dimensionless static pressure change as a function of position (h) throughout the wing's length, with a constant Mach number M = 7 being maintained at different incidence angles. For incidence angles between 5° and 10°, the results show a consistent pressure increase over the length of the wing. In particular, the pressure increases between 5° and 10° incidence angles, from location 0.2 to 0.5. On the other hand, at incidence angles between 15° and 25°, the pressure stays constant between locations 0.2 and 0.5. Above 0.5, the pressure falls from 0.4 to 0.5 and then stabilizes for all incidence angles from 0.6 to 1.0.

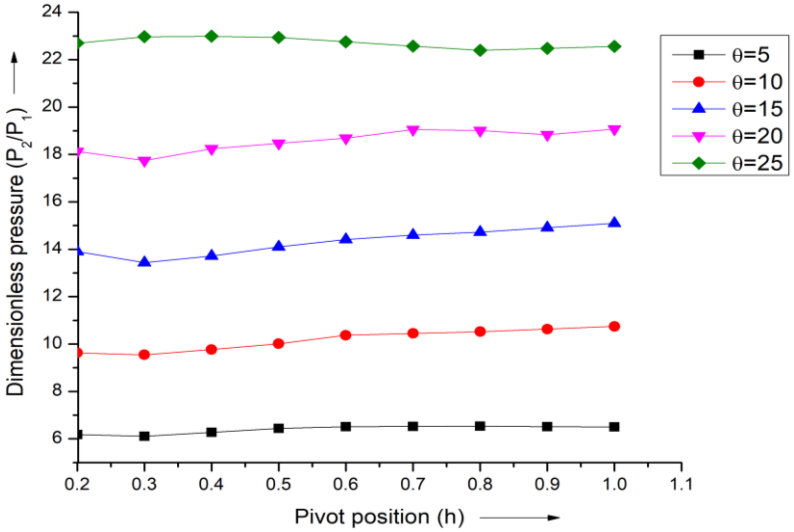

Fig. 13. Dimensionless pressure variation along the pivot position (h) at M = 7

3.5 Surface Pressure at Constant Angle of Incidence at Different Points Along the Wing's Length

ANSYS software has provided the CFD study findings for pressure at several points along the wing's pivot position (h), all while keeping the angle of incidence constant. Figure 14 shows the variations in dimensionless static pressure concerning position (h) along the pivot point of the wing at a fixed angle of incidence (θ = 5°) for various Mach values. For Mach numbers 4.3, 4.8, and 5.5, the results show a constant pressure rise along the 3D wing's pivot point from a location 0.2 to 0.4.

Interestingly, at Mach number 7, the pressure change is noticeable at every point along the wing's pivot position. However, from location 0.5 to 1.0, marginal pressure changes are seen for all Mach numbers along the 3D wing's length.

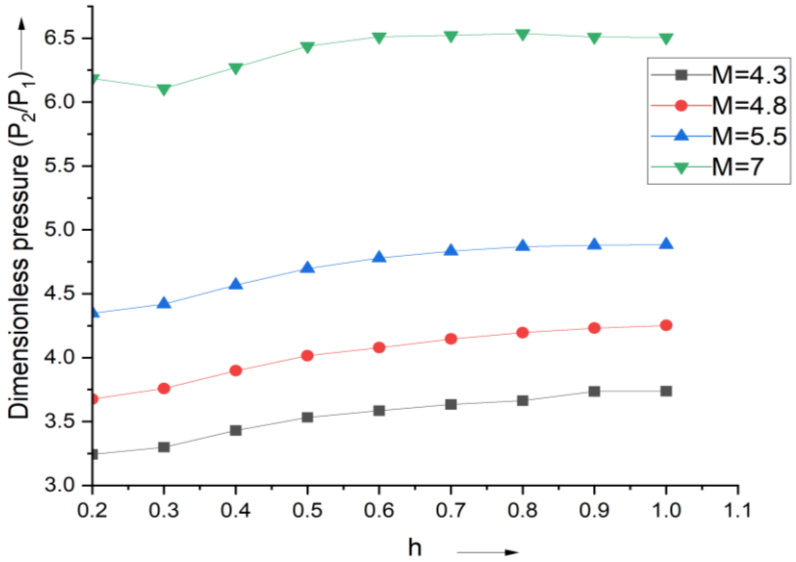

Fig. 14. Dimensionless pressure variation along the pivot position (h) at θ = 5^0

The variation of the dimensionless static pressure with location (h) along the pivot point of the wing at a fixed angle of incidence θ = 10° for different Mach values is depicted in Figure 15. For Mach numbers 4.3 and 4.8, the data show a steady rise in pressure along the wing's pivot position, from location 0.2 to 0.1. Furthermore, a notable reduction in pressure variation for Mach number 5.5 is noted from position 0.2 to 0.3 along the 3D wing's pivot position, succeeded by an increase from 0.4 to 1. The pressure increases from site 0.2 to 0.6 for Mach number 7, and then there are slight fluctuations in pressure from location 0.5 to 1.0 along the wing's length. This change is attributed due the shock strength. The variation of the surface pressure with an increase in the Mach number will diminish and later become independent of the Mach number.

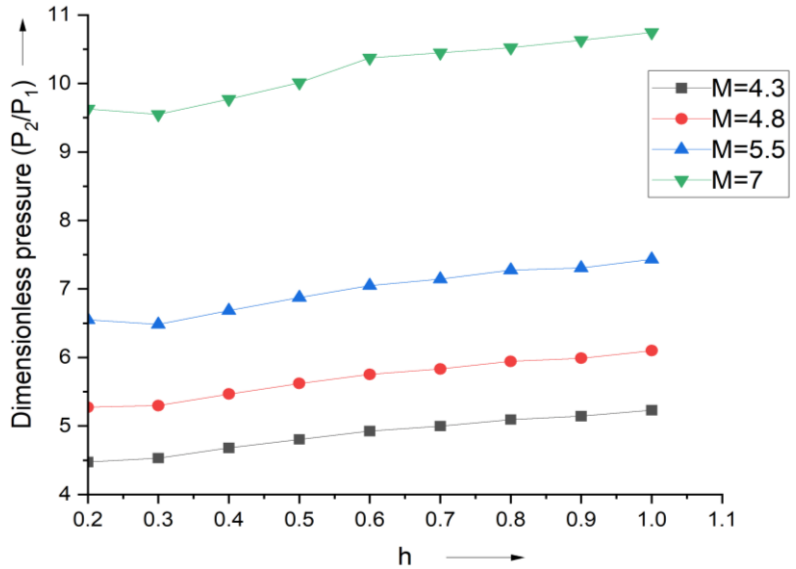

Fig. 15. Dimensionless pressure variation along the pivot position (h) at θ = 10^0

Figure 16 shows the dimensionless static pressure variations along the wing's pivot position at a constant angle of incidence (θ = 15°) for various Mach numbers. Plotting of the normalized surface pressure versus pivot location (h) is done. The findings indicate a consistent increase in pressure along the wing's pivot position, from location 0.2 to 1.0, for Mach numbers 4.3 and 4.8. Furthermore, for Mach numbers 5.5 and 7, a notable increase in pressure variation is noted from location 0.2 to 0.8 along the wing's pivot position. Marginal fluctuations in pressure are found along the wing from location 0.6 to 1.0 for all Mach values.

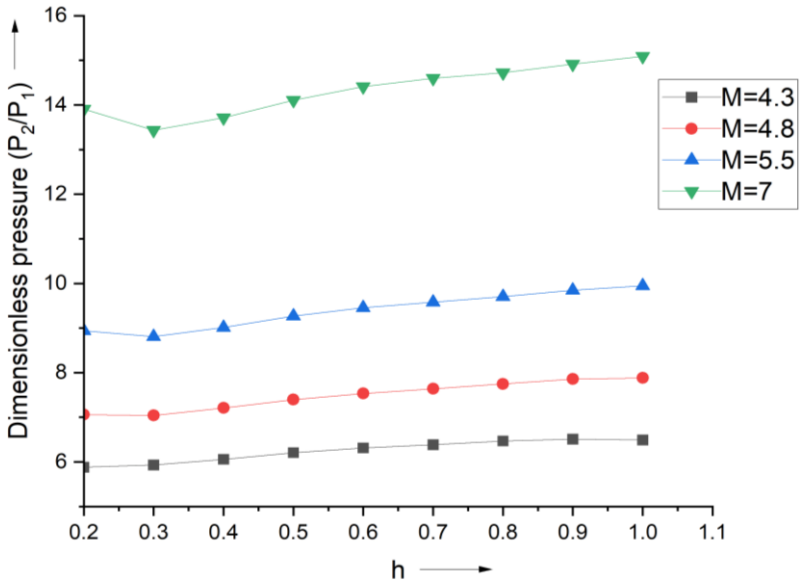

Fig. 16. Dimensionless pressure variation along the pivot position (h) at θ = 15^0

The dimensionless static pressure fluctuations for different Mach values are depicted in Figure 17, concerning position (h) at the 3D wing's pivot point, at a constant angle of incidence (θ = 20°). The results indicate that for Mach numbers 4.3, 4.8, and 5.5, there is an increase in pressure along the wing's pivot position from location 0.2 to 0.4. Furthermore, it is noted that at Mach number 7, pressure drops from location 0.2 to 0.3 before suddenly increasing. The pressure fluctuation is much larger at positions 0.3 to 0.7 on the pivot of the wing. For any Mach number, the pressure slightly varies from position 0.4 to 1.0 along the wing's length.

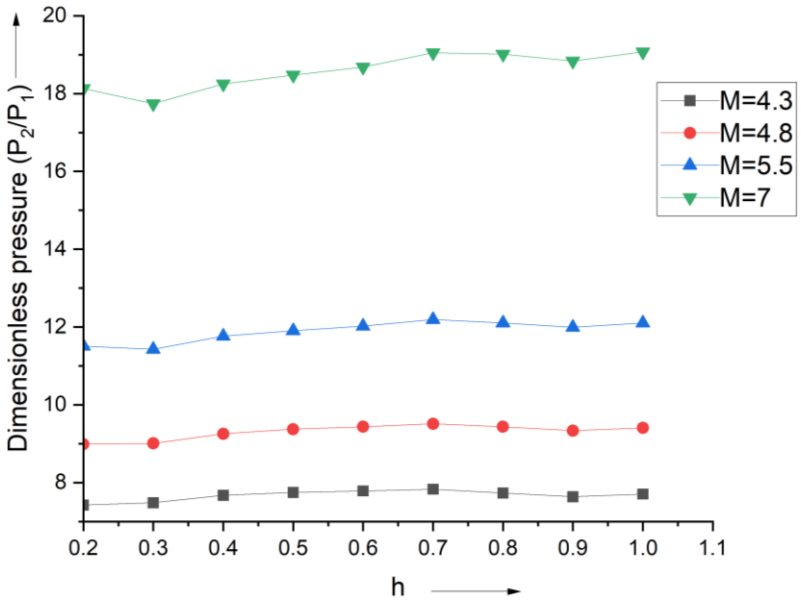

Fig. 17. Dimensionless pressure variation along the pivot position (h) at θ = 20^0

Figure 18 displays the variations in the dimensionless static pressure for various Mach numbers as a function of location (h) along the wing's pivot point at a constant angle of incidence θ = 25°. According to the data, pressure rises for Mach numbers 4.3, 4.8, and 5.5, 7, at the wing's pivot point from location 0.2 to 0.3, and then falls for all Mach numbers from location 0.3 to 1.

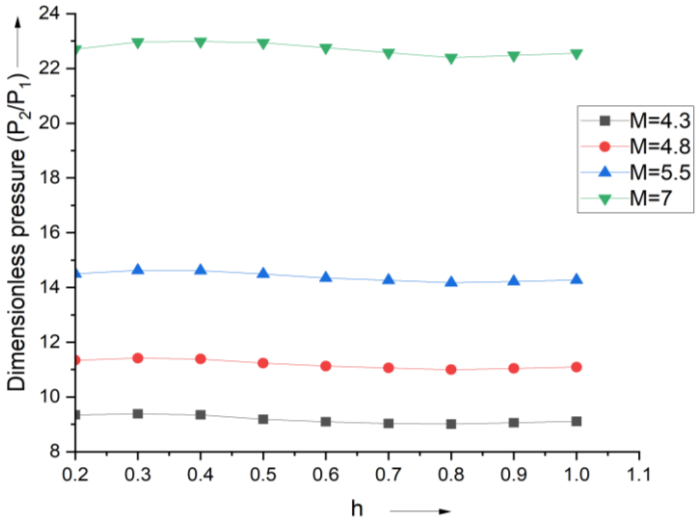

Fig. 18. Dimensionless pressure variation along the pivot position (h) at θ = 25^0

4. Conclusions

The findings presented show that there are several uses for this type of work in the aerospace and defense sectors, particularly when it comes to factors like static pressure, static temperature, angle of incidence, and Mach number along the length of a wing. At hypersonic Mach numbers, aerodynamic heating is the major issue. When the Mach number is greater than five the air which is a non-reacting flow becomes a reacting flow. The demonstrated findings highlight their relevance and applicability within the realms of defense and aerospace technologies. Understanding the

behavior of a wing under different conditions is crucial for designing and optimizing aerospace vehicles. Studies show that when the angle of incidence and Mach number rises, so does the static pressure. Additionally, the study shows that variations in surface pressure on the wing are influenced by both Mach number and angle of incidence. The analytical results obtained through CFD analysis exhibit excellent agreement with the findings of the existing literature. The current investigation generates a database. As such conducting wind tunnel tests is not financially viable. Hence at the initial design stage, these results will be handy, and once the design is finalized based on the analytical and simulation results, one can go for wind tunnel tests resulting in considerable savings.

Acknowledgment
We express our sincere gratitude to Nitte Meenakshi Institute of Technology management for their constant encouragement during our research.

References

[1] Hui, Wai How. "Stability of oscillating wedges and caret wings in hypersonic and supersonic flows." *AIAA Journal* 7, no. 8 (1969): 1524-1530. https://doi.org/10.2514/3.5426
[2] Hui, Wai How. "Interaction of a strong shock with Mach waves in unsteady flow." *AIAA Journal* 7, no. 8 (1969): 1605-1607. https://doi.org/10.2514/3.5441
[3] Liu, D. D., and W. H. Hui. "Oscillating delta wings with attached shock waves." *AIAA Journal* 15, no. 6 (1977): 804-812. https://doi.org/10.2514/3.7371
[4] Hui, W. H. "Supersonic and hypersonic flow with attached shock waves over delta wings." *Proceedings of the Royal Society of London. A. Mathematical and Physical Sciences* 325, no. 1561 (1971): 251-268. https://doi.org/10.1098/rspa.1971.0168
[5] Lighthill, Mo J. "Oscillating airfoils at high Mach number." *Journal of the Aeronautical Sciences* 20, no. 6 (1953): 402-406. https://doi.org/10.2514/8.2657
[6] Ghosh, Kunal, and Binoy Krishna Mistry. "Large incidence hypersonic similitude and oscillating nonplanar wedges." *AIAA Journal* 18, no. 8 (1980): 1004-1006. https://doi.org/10.2514/3.7702
[7] Ghosh, Kunal. "Hypersonic large-deflection similitude for oscillating delta wings." *The Aeronautical Journal* 88, no. 878 (1984): 357-361. https://doi.org/10.1017/S0001924000020868
[8] Hui, W. H., M. F. Platzer, and E. Youroukos. "Oscillating supersonic/hypersonic wings at high incidence." *AIAA Journal* 20, no. 3 (1982): 299-304. https://doi.org/10.2514/3.7914
[9] Ghosh, Kunal. "Hypersonic large-deflection similitude for quasi-wedges and quasi-cones." *The Aeronautical Journal* 88, no. 873 (1984): 70-76. https://doi.org/10.1017/S0001924000020236
[10] Bashir, Musavir, S. A. Khan, Qummare Azam, and Ayub Ahmed Janvekar. "Computational and analytical investigation of aerodynamic derivatives of similitude delta wing model at hypersonic speeds." *International Journal of Technology* 8, no. 3 (2017). https://doi.org/10.14716/ijtech.v8i3.6319
[11] Khan, Sher Afghan, Abdul Aabid, and C. Ahamed Saleel. "CFD simulation with analytical and theoretical validation of different flow parameters for the wedge at supersonic Mach number." *International Journal of Mechanical and Mechatronics Engineering* 1 (2019).
[12] Kalimuthu, R., R. C. Mehta, and E. Rathakrishnan. "Measured aerodynamic coefficients of without and with spiked blunt body at Mach 6." *Advances in Aircraft and Spacecraft Science* 6, no. 3 (2019): 225-238.
[13] Zuhair, Mohammed A. Ba, and A. Mohammed. "Trailing edge geometry effect on the aerodynamics of low-speed BWB aerial vehicles." *Advances in Aircraft Spacecraft Science* 6, no. 4 (2019): 283-296.
[14] Meng, Yu-shan, Li Yan, Wei Huang, Chen Ji, and Jie Li. "Coupled investigation on drag reduction and thermal protection mechanism of a double-cone missile by the combined spike and multi-jet." *Aerospace Science and Technology* 115 (2021): 106840. https://doi.org/10.1016/j.ast.2021.106840
[15] Shaikh, Javed S., Krishna Kumar, Khizar A. Pathan, and Sher A. Khan. "Analytical and computational analysis of pressure at the nose of a 2D wedge in high speed flow." *Advances in Aircraft and Spacecraft Science* 9, no. 2 (2022): 119-130.
[16] Shabana, Aysha, Asha Crasta, Sher Afghan Khan, Abdul Aabid, and Muneer Baig. "Computation of stiffness and damping derivatives of an ogive in a limiting case of Mach number and specific heat ratio." *Fluid Dynamics & Materials Processing* 19, no. 5 (2022): 1249-1267. https://doi.org/10.32604/fdmp.2023.023158

[17] Shaikh, Javed S., Krishna Kumar, Khizar A. Pathan, and Sher A. Khan. "Computational Analysis of Surface Pressure Distribution over a 2D Wedge in the Supersonic and Hypersonic Flow Regimes." *Fluid Dynamics & Materials Processing* 19, no. 6 (2023). https://doi.org/10.32604/fdmp.2023.025113
[18] Pathan, Khizar Ahmed, Prakash S. Dabeer, and Sher Afghan Khan. "Investigation of base pressure variations in internal and external suddenly expanded flows using CFD analysis." *CFD Letters* 11, no. 4 (2019): 32-40.
[19] Pathan, Khizar A., Sher A. Khan, N. A. Shaikh, Arsalan A. Pathan, and Shahnawaz A. Khan. "An investigation of boat-tail helmet to reduce drag." *Advances in Aircraft and Spacecraft Science* 8, no. 3 (2021): 239-250.
[20] Shaikh, Javed S., Krishna Kumar, Khizar A. Pathan, and Sher A. Khan. "Computational Analysis of Surface Pressure Distribution over a 2D Wedge in the Supersonic and Hypersonic Flow Regimes." *Fluid Dynamics & Materials Processing* 19, no. 6 (2023). https://doi.org/10.32604/fdmp.2023.025113
[21] Khan, Sher Afghan, and E. Rathakrishnan. "Active control of base pressure in supersonic regime." *Journal of Aerospace Engineering, Institution of Engineers, India* 87 (2006): 1-8.
[22] Kanaani, Osamah Othman, Sami Abdelrahman Musa Yagoub, Shabir Habib, Akmal Aulia, and Bonavian Hasiholan. "Prediction of gas coning in hydrocarbon reservoir using tNavigator." *Progress in Energy and Environment* 18 (2021): 1-22. https://doi.org/10.37934/progee.18.1.122